HOTVOLC: the official French satellite-based service for operational monitoring and early warning of volcanic ash plumes

Yannick Guéhenneux, Mathieu Gouhier

HOTVOLC: The official French satellite-based service for operational monitoring and early warning of volcanic ash plumes

Yannick Guéhenneux

yannick.guehenneux@uca.fr

OPGC: Observatoire de Physique du Globe de Clermont-Ferrand https://orcid.org/0000-0002-0318-9713

Gouhier Mathieu

Observatoire de Physique du Globe de Clermont-Ferrand

Research Article

Keywords: volcanic ash, volcanic clouds, VAAC, satellite, HOTVOLC, risk, MSG (Meteosat Second Generation)

Posted Date: August 7th, 2023

DOI: https://doi.org/10.21203/rs.3.rs-3210321/v1

Version of Record: A version of this preprint was published at Bulletin of Volcanology on March 7th, 2024. See the published version at https://doi.org/10.1007/s00445-024-01716-w.

HOTVOLC: The official French satellite-based service for operational monitoring and early warning of volcanic ash plumes

Guéhenneux Yannick[1,*] and Gouhier Mathieu[1]
[1] CNRS, IRD, OPGC, Laboratoire Magmas et Volcans, Université Clermont Auvergne, 63000 Clermont-Ferrand, France
[*] Correspondence: yannick.guehenneux@uca.fr

Abstract

Early detection of volcanic ash clouds is crucial to aviation safety and airspace surveillance. With the increase in air traffic and the frequency of volcanic eruptions, the need for effective warning procedures and improved detection methods has become obvious. The eruption of the Eyjafjallajökull volcano in 2010 showed that air traffic operations were severely disrupted, and highlighted the importance of effective communication strategies between stakeholders. To improve monitoring capabilities, satellite techniques have become essential due to their wide coverage and rapid response. This article presents the HOTVOLC 3.0 web-GIS interface, an enhanced version of the CNRS-INSU-certified French operational monitoring platform developed at the Observatoire de Physique du Globe de Clermont-Ferrand (OPGC). By integrating data from the METEOSAT second generation (MSG) satellites, HOTVOLC 3.0 enables early detection of volcanic activity and monitoring of ash plumes and clouds. The HOTVOLC service is designed to support volcanic observatories, volcano research institutes, Volcanic Ash Advisory Centers (VAAC) and other operational actors who play a crucial role in decision-making and the implementation of effective risk management strategies for aviation safety. After a description of how the system works, we provide details of the updated web interface, which enhances the user experience by offering an interface with an operational mode and an archive mode, enabling easy access to past eruptions for training purposes. In the second part we look at the various ash-related observation products (detection algorithms and quantitative products) that are disseminated via the new interface. Finally, we explore future developments of the platform, including the use of machine learning for ash detection, the integration of data from other geostationary satellites to improve product quality, and the forthcoming arrival of data from METEOSAT Third Generation (MTG) satellites.

Keywords

volcanic ash; volcanic clouds; VAAC; satellite; HOTVOLC; risk; MSG (Meteosat Second Generation)

Introduction

Early detection of volcanic ash clouds has become an important objective for the volcanological community, as well as for civilian and military air space monitoring communities. Due to the increase of air traffic levels, volcanic ash clouds were predicted to be a major source of risk to aviation (Casadevall, 1994a; Casadevall, 1994b; Casadevall et al., 1996; Miller & Casdevall, 2000; Prata, 2009; Prata & Tupper, 2009). Indeed, every day there are about 100,000 commercial flights on Earth and there are on average 80 volcanic eruptions every year. Since 1953, there have been about 150 incidents related to aircrafts encountering volcanic ash plumes, of which 26 can be considered severe, although no fatalities have been reported (Lechner et al., 2018). These data dramatically illustrate the current need for monitoring explosive volcanoes and the implementation of efficient warning procedures. The ultimate goal being to reduce to an absolute minimum the hazards posed by volcanic ash drifting into air routes (Casadevall et al., 1999; Guffanti et al., 2005). The major disruption of air traffic operations associated with the loss of billions of Euros caused by the April-May 2010 eruption of Eyjafjallajökull volcano (Iceland), has recently highlighted the importance of developing and improving methods of detection and quantification of volcanic ash, establishing consistent ash concentration threshold and defining safe levels of aircraft engine exposure to ash (International Volcanic Ash Task Force, 2010; Schultz, 2012). But this crisis also highlighted the importance of the communication strategy between the different stakeholders. This includes the implementation of standardized formats (i.e., VONA, Sigmet, Notam, VAA/VAG) and facilitated access to real-time data through web-GIS interfaces, which provides high value-added Earth Observation (EO) products for VOs (Volcano Observatories), VRI (Volcano Research Institute) as well as for end-users (VAACs, Governments, Civil Aviation Agencies, etc.). The latter eruption has raised awareness of the vulnerability of our modern and globalized society to volcanic eruptions and has led to major progress in air traffic risk management (ICAO EUR/NAT VACP, 2016). In particular thanks to the work carried out with the two VAACs (London and Toulouse) in the framework of EuroVolc, a consortium bringing together European actors working on these issues.

VAACs (Volcanic Ash Advisory Centers) are in charge for providing Volcanic Ash Advisories (VAA) and Graphics (VAG) to assist air traffic management in preventing and reducing the risks associated with the atmospheric dispersion of volcanic ash. VAA contain text information such as the aviation color code, time and location of eruption start, VONA and satellite sources, etc. VAG are qualitative contamination maps showing contour lines for different flight levels. In addition, some VAACs provide forecast quantitative contamination charts using VATD (Volcanic Ash Transport and Dispersion) models. In these charts, ash concentrations related to agreed thresholds are provided at various flight levels (Beckett et al., 2020). Usually, the ash plumes take only a few tens of minutes to reach the altitude of long-haul flights, and, according to ICAO requirements, VAACs have 20 minutes after volcanic ash evidence to provide the first VAA/VAG. The reaction time of the VAACs depends mainly on the on-site volcano observatory that must timely provide a VONA (Volcano Observatory Notices for Aviation) with critical information about the on-going activity and input parameters. On some volcanoes, where there are no observatories or where the available monitoring means are scarce, sending a VONA is difficult or even impossible. In this case, the use of GEO satellites is particularly relevant and makes it possible to trigger the volcanic alert and provide the input parameters of the VATD models run by the VAACs. This is the case for example, of the Toulouse VAAC (Météo-France) which relies on data from the HOTVOLC monitoring system (Gouhier et al., 2016; Gouhier et al., 2020) using Meteosat satellite data.

Operational monitoring of volcanic ash in the atmosphere is achieved through both in-situ and remote sensing methods (Gouhier et al., 2012). However, in many cases, the installation of ground stations, the maintenance of expensive instruments and the difficulty of access to erupting volcanoes make the use of satellite-based techniques mandatory (Furtney et al., 2018). But the operational monitoring

from space can rarely be used to predict an eruption by analyzing and interpreting warnings signals (ground displacements, pre-eruptive degassing). Therefore, in the absence of early warnings, the objective is to detect as quickly as possible an anomaly, such as hot spot reflecting the arrival of lava at the surface (Wright & Flynn, 2003), or the formation of gas and ash plume from the vent (Pergola et al., 2008; Rix et al., 2009; Gouhier, 2022). In that aim the use of Geostationary Earth Orbit (GEO) satellite data is mandatory to early detect and track volcanic ash plumes and clouds (Prata & Kerkmann, 2007; Francis et al., 2012; Labazuy et al., 2012; Pavolonis et al., 2020; Gouhier et al., 2020). The need for rapid detection of eruptive events is all the more important as it takes only a few tens of minutes for an ash plume to reach the tropopause, an altitude at which most long-distance flights are operated, which makes the use of GEO satellite even more relevant (Scollo et al., 2009). From a quantitative assessment point of view, there are also many algorithms allowing the calculation of volcanic ash concentration in clouds. Most of them use the thermal infrared waveband, which allows an evaluation during day and night, which is essential for real-time monitoring. We can mention the historical two-band algorithm (Prata, 1989a; Prata, 1989b), which is subject to numerous biases in the detection of pixels containing ash (Simpson et al., 2000; Guéhenneux et al., 2015). As a result, many others studies have led to the development of new detection algorithms such as: the Robust Satellite Technique (Tramutoli, 1998; Pergola et al., 2001; Pergola et al., 2004), the MIR band method (Ellrod & Connel, 1999; Mosher, 2000; Ellrod et al., 2003), the atmospheric correction (Prata & Grant, 2001; Yu et al., 2002), the VIS-IR daytime method (Pavolonis et al., 2006) or more recently the 3-Band method (Pavolonis, 2010; Pavolonis & Sieglaff, 2012; Francis et al., 2012; Guéhenneux et al., 2015).

All this work remains useless to the community if real-time data are not made available to operational actors such as VAACs or volcanological observatories. In this aim we developed in 2010 the HOTVOLC web-GIS interface for easy access to high-value EO products using data from the Meteosat GEO satellite (https://hotvolc.opgc.fr). HOTVOLC is a certified service since 2012 by the CNRS-INSU and it is part of the National Volcanological Observation Service (SNOV). Today, there are only 2 open-access platforms allowing operational quantitative assessment of volcanic ash: (i) the HOTVOLC platform developed by the Observatoire de Physique du Globe de Clermont-Ferrand (OPGC) and allowing quantitative retrieval of both volcanic ash and lava (Gouhier et al., 2016) for 12 volcanic zones (Figure 1) ; and (ii) the Volcanic-Cloud-Monitoring platform from the NOAA-CIMSS (Pavolonis et al., 2018) allowing ash to be detected and tracked using artificial intelligence software (VOLCAT). In this article we will describe the new HOTVOLC 3.0 interface which is a major upgrade from the previous version. This concerns several development axes including the incorporation of new satellites for remote targets from the nadir of Meteosat such as GOES-East for volcanoes in the French West Indies, the development of new ash detection algorithms, and completely redesign user interface with an operational mode and an archive mode. The objective of this new interface is to further facilitate access to real-time data for operational actors, but also facilitate past eruptions access that can be used for training purposes.

1. HOTVOLC 3.0: A major web-service upgrade for improved crisis response

1.1. Acquisition station, processing module and storage system hardware design

In order to be able to provide the stakeholder community with Earth observation products for decision support, in near-real time, we had to equip ourselves with a satellite data reception station. This was made possible by the signature of a tripartite agreement between EUMETSAT (the European consortium in charge of the production and dissemination of satellite data), MétéoFrance (the French national agency for meteorology and weather forecasting) and the Observatoire de Physique du Globe de Clermont-Ferrand (the research infrastructure hosting the HOTVOLC service). This agreement

authorizes HOTVOLC to use data from the METEOSAT SECOND GENERATION weather satellites by removing the 24-hour embargo on the data and providing access to the EUMETSAT direct broadcast service via a decryption key.

The first version of the MSG data reception station installed at the OPGC was released in January 2009. Its system is composed of four different modules: [1] the data acquisition system, [2] the data processing module, [3] the archiving system and [4] the webcasting server.

1.1.1. The acquisition system

This system is dedicated to the reception of data from geostationary satellites and is composed of:

- A 110 cm dish installed on the roof of the OPGC.
- A receiver.
- Two DVB demodulation cards, which will demodulate the analog signal received by the dish into a digital signal.
- An acquisition PC
- A decoding key provided by EUMETSAT
- Tellicast software provided by EUMETSAT

This system only supports the first level of reception and does not evolve much after its installation. The system receives the frames from the antenna, assembles the segments and decrypts them using the EUMETSAT key. These segments are then sorted and transmitted to the processing module. This system can, to a limited extent, supervise its own operation. If no data is received for three minutes, the receiving application resets, and if it fails, the system is automatically restarted.

1.1.2. The processing module

This module is where all the processing is carried out before the data is archived. It is composed of:

- A multiprocessor server computer
- A local archive (3TB)
- The SatNAP software
- The HOTVOLC processing software

The SatNAP (Satellite Near Archive Processing) software was developed within the framework of the "Meteosat Second Generation vers une Acquisition Temps-Réel" French research group (GDR MSG-ATR). It is an open-source software written in C language and designed to exploit the data stream from an MSG acquisition system. It allows the management of the reception stream by ensuring: [1] the decompaction of the data and the management of the missing segments, [2] the sorting of the data stream, and [3] the recompression of the data in a standardized raw format.

The HOTVOLC processing software, described below in section XX, is written in Python and aims at extracting and automatically processing areas of interest in the data to provide advanced products such as radiance maps, thermal anomaly maps, volcanic ash maps or time series.

Once the processing is completed, the data are sent to the archiving system.

1.1.3. The archiving system

The archiving system stores all the MSG scenes acquired by the OPGC receiving station since 2010, as well as GeoTIFFs and map server tiles from HOTVOLC products.

It is made up of DELL storage bays configured as a SAN system (storage area network) in RAID 5 for a usable storage capacity of 200 TB. The system is hosted in the data center of the Université Clermont Auvergne, which has the necessary security infrastructures, such as a dual power supply, heat flow management, etc.

1.1.4. The webcast server

Adjacent to the processing module, this LAPP-type server (Linux, Apache, PostgreSQL and PHP) manages the HOTVOLC data web distribution interface (described below) and the web services for their broadcasting to the EPOS platform (European Plate Observing System). It uses the processing module's local archive (3 TB) to store the latest GeoTIFFs and map tiles of the HOTVOLC products and has access to data stored on the archive system via Network File System (NFS) mounts. This server also houses the relational database running PostgreSQL.

1.1.5. Hardware design evolution

The installation, in the first half of 2023, of a second acquisition station represents a major evolution of the system. This new antenna is currently being used to evaluate the reception and integration of GOES data, which should improve the quality of the HOTVOLC service for volcanoes in the French West Indies. In a second phase, it will enable the first reception station to be completely renovated without interruption of service. The antenna of the first acquisition station is beginning to suffer from the effects of time, its braking system is starting to play up and the signal-to-noise ratio is slowly deteriorating. This renovation, and the doubling of the acquisition system, is an opportunity to increase the quality of HOTVOLC's services by significantly reducing failures in the reception of data streams from EUMETSAT and therefore the number of missing data in the database.

1.2. Processing software design

The processing software is the main tool of the HOTVOLC system, and its purpose is to read an MSG scene and produce the ten or so Earth observation products for the twelve defined zones of interest: [1] Iceland, [2] France, [3] Italy-Greece, [4] African Rift, [5] East Africa, [6] Comoros, [7] Reunion Island, [8] Cameroon, [9] Cape Verde, [10] Canary Islands, [11] Azores, [12] West Indies (Figure 1). This software, written in Python 3 with an object-oriented design, was guided by a strong time constraint, since all processing had to take place within the 2.5 minutes separating two successive MSG acquisitions. The software, launched automatically every 15 minutes via the "crontab" task scheduler, takes place in 4 steps:

The first step is to create a "full globe" scene by collecting the 8 segments that make up a whole image, for the 6 spectral bands used to create the various products: 3.9 µm, 7.3 µm, 8.7 µm, 10.8 µm, 12 µm and 13.4 µm. These 6 "full globe" images are then converted from digital count to effective radiance (in $mW.m^{-2}.sr^{-1}.(cm^{-1})^{-1}$) using the calibration coefficient and calibration offset. And finally converted to brightness temperature (in Kelvin) through an analytical relationship suggested by the Planck spectral function (Schmetz et al., 2002). The twelve volcanic zones are then extracted from the global scene, and the rest of the program is multithreaded, running simultaneously for all 12 extracted zones.

The second stage, which applies simultaneously to each of the volcanic zones, begins with the management of any missing data that might prevent the rest of the program from running smoothly.

Once this check has been completed, the program begins creating the various earth observation products. The different products are created successively in the following order:

- A colored composition called RGB using spectral bands at 8.7 µm, 10.8 µm and 12 µm (see section 2.4).
- The two cloud products, starting with an 8-level cloud temperature classification, which is followed by a cloud height product using a look-up table.
- Volcanic ash detection products using the 2-band algorithm (see section 2.1) and its derivatives ash cloud altitude (see section 2.5), ash plume concentration (see section 2.6) and volcanic ash cloud contour (see section 2.7).
- Volcanic ash detection product based on the 3-band algorithm (see section 2.2).
- The volcanic ash detection product based on the 5-band algorithm (see section 2.3).

At this level, the data are converted from brightness temperature to spectral radiance following Planck's law, and the last three products are created:

- A reported SO2 product based on the spectral luminance difference between the spectral bands at 8.7 µm and 10.8 µm.
- The product of the thermal state at 3.9 µm and the product of thermal anomalies detected using the normalized thermal index (Gouhier et al., 2016).

In the third step, GeoTIFFs, in satellite projection, of all products are created and archived, then reprojected in flat square projection for viewing on the web interface. Once reprojected, the map server tiles are created using “gdal2tiles.py”. This is the software's most time-consuming action, and is itself multithreaded since tiling is carried out in parallel for each GeoTIFF.

The fourth and last step is to save all the information collected and created in the previous steps: metadata, time series, etc., in the database.

1.3. Web-GIS interface design

1.3.1. The original philosophy: real time diffusion

HOTVOLC's first web interface was launched in the spring of 2010, during the crisis caused by the eruption of Eyjafjallajökull. The initial objective was to provide the French Ministry of Ecology, Energy, Sustainable Development, and the Sea (MEEDEM) with near-real-time estimates of quantitative parameters constraining the dynamics of ash plumes from the vent to the atmosphere (Labazuy et al., 2010). It was this philosophy of real-time dissemination of earth observation products that guided the development and design of the second version of HOTVOLC's web interface, available for over 10 years and which has enabled HOTVOLC to be a CNRS-INSU-certified service since 2012.

This interface (Figure 2) provides instant information on the level of activity of the various volcanoes monitored, the color of the marker depending on the thermal activity observed at the volcano (white - no activity, green - low activity, yellow - medium activity and red - high activity). Clicking on a volcano marker takes you directly to the latest observation data. The lower part of the left-hand menu lets you select the products to be displayed, while the upper part, with its calendar, lets you navigate through time. Finally, a button on the top-right banner of the interface gives access to a dozen different time series, such as the thermal state of the volcano at 3.9 µm and 12 µm, the number of thermal anomalies, the total spectral luminance in the event of an eruption, the lava volume flow rate (only for Etna and Piton de la Fournaise), the area of ash or SO2 plumes, or the altitude and maximum ash concentration of plumes.

After more than ten years in operation, the HOTVOLC database has been enriched by nearly a hundred different eruptions. And the design of the web interface has begun to show its limitations. Designed to take advantage of real-time MSG data acquisition, it proved impractical for exploring the database of previous eruptions. That is why we started developing the version 3 of the HOTVOLC web interface.

1.3.2. An upgrade to take advantage of HOTVOLC's extensive database

The idea behind the design of this V3 was to retain the HOTVOLC service's core strength of real-time broadcasting, while making it easy for users to take advantage of and explore the eruption database built up over the years. The choice was therefore made to divide the interface into two modes with the same feel and look, to make the user experience as simple as possible. A switch on the top left of the interface allows you to toggle between the two modes (Figures 3 and 4).

1.3.2.1. The two interface modes

The first variant of the interface, which is the one you arrive at by default, focuses on real time (Figure 3). For the user, apart from a few cosmetic adjustments, operation is identical to the V2 interface described above. The latest observation data can be accessed directly by selecting a volcano. Navigation in time is limited to a 2-year buffer; to explore older data, you need to switch to the second interface.

The second mode of the interface (Figure 4) focuses on exploring the archive of eruptions recorded by HOTVOLC. This mode offers the user two possibilities for searching and discovering eruptions: [1] click on a volcano's marker or [2] use the advanced search form (Figure 4.a). Clicking on a volcano marker will take you directly to the last eruption recorded for that volcano, and a list of all eruptions for that volcano will appear in tabular form in the left-hand menu (Figure 4.b). The advanced search form allows to enter four search criteria: a start date, an end date, an area of interest and a volcano. The search result is displayed as a table directly below the search form. Any eruption can be viewed and explored by clicking on the corresponding row in the results table.

One of the major changes in the way the interface works in archive mode concerns time navigation. The calendar has disappeared from the left-hand menu and is replaced by a timeline at the bottom of the interface, covering the entire eruption period (Figure 5). The date is selected either by filling in the form field, using one of the four buttons to increment or decrement the time by 15 min or hour, or by clicking on the timeline. You can zoom the timeline using the mouse wheel and navigate back and forth by dragging the mouse while holding down the CTRL key on the keyboard.

1.3.2.2. Addition and rework of features and consequences of technical changes

This interface update was an opportunity to complete and add functionalities to enhance the user experience. For example, the use of directional arrows while holding down the CTRL key, to increment or decrement time by 15 minutes (right and left arrows) or 1 hour (up and down arrows); or the ability to CTRL + click on a point in a time series to move directly to the corresponding date.

A complete overhaul of the measurement and annotation tools, which were not very functional in the previous version, means that true GIS functionality can now be added directly to the interface (Figure 6). Users can now easily draw and edit markers, circles, lines and polygons, add text annotations and, above all, measure distances and areas. This makes it possible to create annotated figures on the fly, which can be an invaluable aid when writing reports.

Finally, an internal tool for generating a unique URL will be made public and added to the interface. This tool allows you to generate an html link that points directly to a volcano, at a defined date and on a specific product (GeoTIFF or time series). This little tool allows the user to save a page of interest to come back to later or to share with others.

From a technical point of view, this new version of the web interface was developed in PHP using the Laravel framework, and in JavaScript. The decision was made to change the library solution for dynamic map display to Leaflet. This has enabled us to take advantage of the technological innovations that have taken place in recent years, and in particular offers us the possibility of removing the map tiling server for the display of GeoTIFFs, in favor of a simple PNG image. As explained in section 1.2, creating the tiles is the most time-consuming stage of the processing. What's more, each additional zoom level leads to the creation of an exponential number of additional files, which had led us to drastically limit the maximum zoom allowed, which could prove frustrating for users. This change will not only improve processing times, but will also mean that zoom levels are no longer limited when browsing the interface.

2. Available EO product for operational stakeholders

As explained in section 1.2, HOTVOLC's web interface provides users with more than a dozen different earth observation products. Two of these relate to cloud cover, with one product providing information on cloud top temperature and the other on cloud altitude. Two other products provide information on the thermal state of volcanoes, with a spectral radiance map at 3.9 µm and a thermal anomaly map. These two products are described in detail in (Gouhier et al., 2016). A fifth is the result of an SO2 detection algorithm. And finally, seven different products concern the detection and quantification of volcanic ash clouds. Among these seven products, describe in details here after, five are detection algorithm and the two others are quantitative products.

2.1. 2-Band algorithm

The historical 2-Band method proposed by Prata (Prata, 1989a; Prata, 1989b) use the differential of extinction properties that affects the absorption and scattering of the upwelling ground radiance by particles. This allows, in the spectral region of the inversion window (11-12 µm), to distinguish silicate particles (i.e., volcanic ash) from other particles such as ice crystals or water droplets. Indeed, Prata (Prata, 1989b) has shown that the Planck brightness difference (BTD) between channel at 11 et 12 µm, defined as $T(\lambda_{11}) - T(\lambda_{12})$ is positive above a cloud of water and/or ice particles ($BTD_{11\text{-}12} > 0$) while it is negative above a cloud of ash particles ($BTD_{11\text{-}12} < 0$). So, with this method a pixel is regarded as containing ash if the following condition is met:

$$Bt_{10.8\,\mu m} - Bt_{12\,\mu m} < 0\,K$$**Error! Reference source not found.Error! Reference source not found.**

This is the first detection index used in HOTVOLC (Figure 7.b), hereafter called “ASH-2” product. Unfortunately, this method suffers well documented limitations (Simpson et al., 2000; Guéhenneux et al., 2015) that may limit its use for automated detection of volcanic ash by leading to [1] an underestimation of the ash cloud size: in moisture rich environments (Rose et al., 2001; Pavolonis et al., 2006), over cold environment, and when the acquisition geometry has a significant zenith angle (Guéhenneux et al., 2015), or [2] an overestimation of the ash cloud: in presence of mineral dust clouds (Ackermann, 1997; Simpson et al., 2000; Watkin, 2003), when thermal relaxation effect occurs above ground during cloudless nighttime conditions (Platt & Prata, 1993), on top of convective clouds that overshoot the tropopause (Potts & Ebert, 1996), and misalignment between the band at 11 and 12 µm to the sensor (Prata et al., 2001; Watkin, 2003).

2.2. 3-Band algorithm

Even if the ASH-2 product is very powerful under the supervision of an informed user, this method is ineffective for automated ash cloud detection. Therefore, more sophisticated techniques have been developed to improve ash characterization such as: the Robust Satellite Technique (Tramutoli, 1998; Pergola et al., 2001; Pergola et al., 2004; Marchese et al., 2011), the MIR band method (Ellrod & Connel, 1999; Mosher, 2000; Ellrod et al., 2003), the atmospheric correction (Prata & Grant, 2001; Yu et al., 2002), the VIS-IR daytime method (Pavolonis et al., 2006) or more recently the 3-Band method (Pavolonis, 2010; Pavolonis & Sieglaff, 2012; Francis et al., 2012; Guéhenneux et al., 2015) which is the second index used in HOTVOLC and referred to the "ASH-3" product.

The ASH-3 product uses two Boolean (true/false) tests based on brightness temperature difference (BTD) and using three thermal infrared channels located at 8.7, 11, and 12 µm (Figure 7.c). The first test is the same as the 2-Band method (Prata, 1989a) using BTD between bands at 11 and 12 µm. The second test use the BTD between 8.7 and 11 µm where ash particles tend to have positive $BTD_{8.7\text{-}11}$ while water/ice particles are characterized by negative values (Guéhenneux et al., 2015). To sum up, pixels contain volcanic ash if the two following conditions are true:

$$Bt_{10.8\,\mu m} - Bt_{12\,\mu m} < T_{cutoff-1} \text{ (with } T_{cutoff-1} \approx 0)$$

$$Bt_{8.7\,\mu m} - Bt_{10.8\,\mu m} > T_{cutoff-2} \text{ (with } T_{cutoff-2} \approx 0)$$

Theoretically $T_{cutoff\text{-}1}$ and $T_{cutoff\text{-}2}$ have to be set at 0 K but due to water vapor, mixed pixel, scattering effect and viewing geometry, values can be in the range -2 to +2 K (Prata & Grant, 2001; Watkin, 2003).

2.3. 5-Band algorithm

The third volcanic ash detection algorithm used by the HOTVOLC system works with five spectral bands. To the 8.7, 10.8 and 12 µm bands, used by the previous algorithms, are added the 3.9 µm and 13.4 µm bands. The addition of these two spectral bands allows respectively to consider the solar contribution within the ash absorption and scattering, for the mid-wave infrared band, and to remove the artifacts related to convective clouds for the band at 13.4 µm (Figure 7.d). The operation of the 5-Band algorithm is divided into two phases: [1] a first phase of very restrictive detection whose objective is to reduce as much as possible the number of false positives by concentrating on the core of the volcanic ash plume and [2] a second phase of detection much more permissive but applying only to the pixels in the vicinity of the pixels flagged in the first phase.

During the first phase the detection follows the same scheme as the 3-Band detection algorithm, the pixels are flagged if they simultaneously meet the two following conditions:

$$Bt_{10.8\,\mu m} - Bt_{12\,\mu m} < -0.5\ K$$

$$Bt_{8.7\,\mu m} - Bt_{10.8\,\mu m} > -0.5\ K$$

However, in order to limit false positives as much as possible, the flagged pixels are not considered and are masked if they meet at least one of the three following conditions:

$$\frac{(Rad_{3.9\,\mu m} - Rad_{12\,\mu m})}{(Rad_{3.9\,\mu m} + Rad_{12\,\mu m})} < Threshold \text{ (night: } 0.042 \text{ | day: } 0.055)$$

$$\frac{(Bt_{8.7\,\mu m} - Bt_{12\,\mu m})}{(Bt_{10.8\,\mu m} - Bt_{13.4\,\mu m})} > -0.05\ K$$

$$\left(\frac{(Bt_{10.8b\mu m} - Bt_{12\,\mu m})}{Bt_{13.4\,\mu m}}\right) \times 100 > -0.35\ K$$

To finish the first phase all the solitary flagged pixels are also masked.

The second part focuses on the pixels closest to those selected in the first phase (within a range of 20 pixels around the flagged pixels) because they are considered to have a high probability of belonging to the ash cloud. The two Boolean tests of the 3-Band algorithm are applied to all these pixels with much more permissive thresholds than usual.

$$Bt_{10.8\,\mu m} - Bt_{12\,\mu m} < -0.25\ K$$

$$Bt_{8.7\,\mu m} - Bt_{10.8\,\mu m} > -2\ K$$

And finally, are masked pixels that meet the following condition because considered to have a very high probability of being artifacts related to thermal relaxation phenomena.

$$\frac{(Rad_{3.9\,\mu m} - Rad_{12\,\mu m})}{(Rad_{3.9\,\mu m} + Rad_{12\,\mu m})} < Threshold\ (\text{night: } 0.042 \mid \text{day: } 0.055)$$

2.4. RGB/24-bits algorithm

All the algorithms presented above use successive tests on a 32-bit monochromatic raster image (floating-points) from the brightness temperature or spectral radiance. These images come from the processing of Meteosat-11 level 1.5 data (native format: 10 bits). In contrast, the algorithm presented here, uses the spectral combination of various waveband (8.7, 10.8 and 12 µm) to build a 3-channel multispectral image (Figure 7.a), usually called RGB, where each channel corresponds to a waveband difference as follows:

$$Red = Bt_{10.8\,\mu m} - Bt_{12\,\mu m}$$
$$Green = Bt_{10.8\,\mu m} - Bt_{8.7\,\mu m}$$
$$Blue = Bt_{10.8\,\mu m}$$

In this configuration, the result obtained is a combination of 3 waveband on a single composite image whose dynamic range is 24 bits (i.e., 8 bits on each of the 3 RGB channels) and allowing a very detailed visualization of the various products which compose the image (Figure 7.a). This method is particularly effective for the discrimination of volcanic ash that appear in dark blue on the image and allowing the detection of ash at threshold as low as 0,1 g/m^2. This color-based detection indicator must now be numerically translated to allow automated detection of ash-bearing pixels. For this purpose, we have defined a succession of tests for the 3 channels (R, G, B) each having a 0-255 dynamic range (i.e., 8-bits), as follows:

Pixels contains volcanic ash if:

$$\text{Test \#1: } \frac{Blue}{Green} > 2$$

$$\text{Test \#2: } Red < 100$$

$$\text{Test \#3: } Green < 100$$

The first test is the most important and allows the detection of the dark blue color, as it appears in the center of the image (Figure 8.a). The second test allows removal of the pink color pixels. In the image, they correspond to the presence of clouds of fine ice crystals of high altitude (type cirrus), which can sometimes pass the first test. A value set at 100/255 allows a reliable elimination of these unwanted particles. Finally, the third test is particularly useful under clear weather. Indeed, in perfectly clear atmospheric conditions, the image appears light blue which can cause serious detection problems if using the first test only. Again, a value set at 100/255 allows the eradication of most unwanted pixels. Figure 8 shows an example of the Nyiragongo eruption in May 2021, during which a weak ash plume was emitted. One can see on Figure 8.a that a dark-blue color ash plume is visible. As an example, we pinpointed the RGB values of a pixel located in the center of the plume, and providing values R=42, G=23 and B=190. With these values, we can clearly see that the selected pixel passes the three tests without any problem. On Figure 8.b, pixels containing ash, i.e., those that pass all the tests, are identified by the color yellow.

As a full-scale test, we tested this technique on the entire explosive phase associated with the May 2021 eruption of Nyiragongo, which extends from about May 23 to July 15. This is a particularly challenging test because the weather is quite bad, and the concentration of ash emitted is rather low. The algorithm was run on about 5000 images (1 every 15 minutes) using 3 different spectral band to recreate at each time step an RGB composite image where each pixel is tested using the procedure described above. From the pixels identified in each image we were then able to use our standard operational procedures (Gouhier et al., 2020) to calculate the mass of ash in the cloud in each image. The result is presented in Figure 9, showing the evolution of the ash load (expressed in kilotons) over time.

2.5. Ash plumes heights

The ash plume height product is an extension of the ASH2 product, providing a critical information for aviation safety. It is based on the use of the CCT method (i.e., Cloud Top Temperature) where the brightness temperature of the cloud surface at 10.8 µm is compared to an atmospheric temperature-altitude profile (theoretical or measured from radio-sounding). For operational purposes, the CCT method used is based on climatic models to derive temperature-altitude profiles. Four different profiles can be used, depending on the latitude of the target and the day of the year (Table 1).

If the target latitude is between -23°S and 23°N, then the tropical profile is used, regardless of the season. For all other latitude values, a mid-latitude profile is used, as follows:

- The day of the year is between 0 and 80 and between 355 and 365:
    - Latitude is less than -23°S, then the summer profile is used.
    - Latitude is greater than 23°N, then the winter profile is used.
- The day of the year is between 80 and 172 or between 264 and 355:
    - Whether the latitude is below -23°S or above 23°N, the mid-season profile is used.
- The day of the year is between 172 and 264:
    - If the latitude is below -23°S, the winter profile is used.
    - If the latitude is above 23°N, the summer profile is used.

Once the correct profile has been identified, for each pixel containing ash, its brightness temperature value at 10.8 µm is compared with the profile entries to obtain the equivalent altitude (Figure 10.b).

The CTT technique can only works for tropospheric emissions since the thermal inversion phenomenon above the tropopause leads to a non-unique solution. Furthermore, it is important to note that this method relies on two critical assumptions: [1] the ash particles must be in thermal equilibrium with the ambient air, and [2] for the cloud temperature to be representative of the true top temperature, the cloud must be optically thick ($\tau > 5$).

2.6. Ash plumes SCD

TIR sensors have proven to be very useful for the operational characterization of volcanic ash cloud. They allow reliable 24/7 detection as demonstrated above from various techniques all using differential extinction properties of silicate particles. Since the 1990s, the quantitative ash concentration was made possible from the inversion of satellite-based TIR data (Prata, 1989a; Wen & Rose, 1994). In that aim, a similar retrieval scheme has been developed and used for HOTVOLC service (Gouhier et al., 2020).

IR imager such as SEVIRI provide plane-parallel (2D) images of the ash cloud, and the mass given in a pixel is an oblique integration of particles loading from the ground to the sensor and usually referred to as slant column densities (SCD). As a result, we can ultimately provide a "surface concentration" of the cloud (Figure 10.c), usually expressed in g/m^2, from the ratio of the total mass over the pixel surface M/S. However, the mass retrieval computing time remains relatively high compared to the METEOSAT acquisition frequency (1 image/15 min).Thus, in the current version of HOTVOLC, look-up tables are pre-computed from the Eddington approximation (Gouhier et al., 2020) for a wide range of standard input parameters (grain size distribution, optical depth, ground brightness temperature, emissivity, refractive index, etc.). Then, slant column densities of ash have been systematically inferred from the inversion of benchmarks case studies (e.g., Etna, Eyjafjallajökull), allowing a simple parameterization of SCD from the ash cloud brightness temperature at 10.8 µm. Therefore, the computation of first order ash SCD is immediate, expressed in g/m2, and of the form:

$$SCD = \alpha \times exp\left(\beta \times Bt_{10.8\ \mu m}\right)$$

where α and β are coefficients obtained by best fit matching, and $Bt_{10.8\ \mu m}$ is the ash cloud top brightness temperature at 10.8 µm on the satellite image.

2.7. Ash contour

The Volcanic Ash Cloud Contour product only applies to a defined area of interest around each volcano, generally a 40 by 40 pixels area centered on the volcano. The first step is to apply the same ash detection test to this search window as for the ASH2 product:

$$Bt_{10.8\ \mu m} - Bt_{12\ \mu m} < 0\ K$$

This produces a 2-dimensional array, containing only 0 (no ash) and 1 (presence of ash) (Figure 11.a), on which we apply a marching squares method (Gong & Newman, 2017) to calculate isovalued contours (Figure 11.b). Finally, we calculate the convex hull around the previously calculated isolines, with a safety distance around the isolines of 3 pixels (Figures 10.a and 11.c). This convex hull is the Ash Cloud Contour product that can be exported in the WKT format.

3. Recommendation for future technical improvements

Since its creation in 2009, with the installation of the MSG data acquisition station, the HOTVOLC service has constantly evolved to offer users not only a better navigation experience, but also new observation and decision support products. We are currently planning three major areas of future technical development. The first concerns the use of machine learning to improve the detection of volcanic ash clouds. The second involves integrating data from other geostationary satellites to improve the quality of products on targets at the edge of the MSG swath. And last but not least, the arrival of the third-generation METEOSAT satellite.

3.1. Machine learning for volcanic ash detection

In over ten years, we have acquired a very substantial database of over 5 million MSG acquisitions covering hundreds of eruptions. One of our major projects in recent years has been to improve the automatic detection of volcanic ash clouds. With 4 different detection algorithms today, each with their own strengths and weaknesses, we need to go further and take advantage of our massive database. The latter should serve as a basis for machine learning work to develop more efficient algorithms. In the years to come, we need to carry out this work with data preparation in order to set up a relevant training set. This will be done by exploring the HOTVOLC eruptive catalog, in order to create a bank of suitable multispectral images. We could also look into the possibility of enriching the training set with synthetic data. The latter could be developed by direct modeling of radiative transfer. The second step will be to test and select the various algorithms to be run. At this stage, we're not ruling out any options: (i) First of all, we'd like to explore the capabilities of supervised learning via logic classification, machine vector or decision tree algorithms. These are simple methods which require less data than the others, but whose prior labeling work can prove tedious and potentially bias the training set. (ii) Conversely, we will test the capabilities of unsupervised learning using k-means clustering algorithms, the aim of which is to explore new relationships between different records (e.g. spectral bands) and reveal common features enabling the efficient clustering of pixels containing ash. This priority work should lead to a significant improvement in decision support for air traffic management in the area covered by the Toulouse VAAC.

3.2. Increase products quality by integrate data from others geostationary satellites

As a CNRS-INSU-certified member of the French National Volcanological Observation Service, one of our priorities is to monitor active French volcanoes in the West Indies (Soufrière de Guadeloupe, Montagne Pelée) and on Reunion Island (Piton de la Fournaise). Unfortunately, these targets are located on the edge of the MSG swath, where the spatial resolution of the pixels is severely degraded. So instead of 3 km by 3 km at nadir, we end up with pixels of around 4 km by 9 km at Antilles level and 3.5 km by 7 km at Piton de la Fournaise. The solution envisaged to improve the quality of our products on these priority targets is to use data from other geostationary satellites.

For the West Indies region, the GOES-16 satellite, positioned at 75.2° West longitude, is the perfect candidate. With a spatial resolution of 2km at nadir and an acquisition frequency of 10 minutes, this satellite offers gains in both spatial quality and temporal resolution. The installation of a second acquisition station in the first half of 2023 has enabled us to assess the feasibility of using GOES data for volcanoes in the French West Indies. Data reception is proceeding smoothly, and an initial integration test of an RGB product produced highly satisfactory results in terms of improved spatial resolution (Figure 12). This required adaptation of the web interface to take account of the different acquisition frequency. Before definitively integrating GOES data into the HOTVOLC system, work is underway to review all product creation algorithms in order to adapt them to the spectral bands of GOES, which are different from those of MSG.

For the Piton de la Fournaise, we are currently looking into the possibility of using data from EUMETSAT's Indian Ocean Data Coverage (IODC) service. This service provides data from the old MSG satellites, which were replaced by their successor and moved to a more easterly orbit to image the Indian Ocean. At present, this service is fed by data from Meteosat 9, the second MSG satellite, located in an orbit at 45.5° East. The advantage of this solution is that it is based on the use of data from identical satellites, so there would be no technical issues in integrating them into HOTVOLC's processing and broadcast chain.

3.3. From METEOSAT Second Generation to METEOSAT Third Generation

The successful launch of the first METEOSAT Third Generation (MTG) satellite on December 13, 2022, and the gradual replacement of second-generation satellites by third-generation ones over the coming decade, will lead to far-reaching changes in the HOTVOLC system. The capabilities provided by the Flexible Combined Imager (Holmlund et al., 2021), SEVIRI's successor, will give us the opportunity to set up much better monitoring of volcano eruptive dynamics. Particularly thanks to the increase in acquisition frequency from 15 to 10 minutes, which will enable us to react more quickly to eruptive events and produce even more detailed time series. The improved spatial resolution, from 3 km to 2 km or even 1 km for the visible spectral bands and those at 3.8 µm and 10.5 µm, will mean an appreciable gain in the quality of earth observation products, with enhanced spatial sensitivity.

From a technical point of view, we don't yet know what modifications we'll need to make to our acquisition system, but the experience we've gained in replacing MSG data for swath-edge targets with data from other geostationary satellites should make it easier to integrate these new data into the web interface.

Conclusion

This article highlights developments and future prospects for the HOTVOLC satellite-based system, which plays a crucial role in real-time monitoring of volcanic activity, and supports the operational management of volcanic crises by volcanological observatories and Volcanic Ash Advisory Centers (VAACs).

Over the years, HOTVOLC has undergone significant advances, most notably with the recent redesign of its web-GIS interface, offering users an improved browsing experience and easy access to a wide range of earth observation products. This recent redesign of the web interface, presented in the first part of the paper, introduces two distinct modes, real-time and archive mode, offering users seamless access to real-time volcanic activity information and a vast database of recorded eruptions. Real-time mode presents instantaneous data on the level of activity of the various volcanoes monitored, giving users access to the latest observation data. Archive mode, meanwhile, provides a powerful tool for exploring the wide catalog of eruptions covered by the HOTVOLC database, thanks to various search options that facilitate discovery. In addition, this web interface update adds enhanced measurement and annotation tools, enabling users to draw, edit and measure on the map, and the integration of the Leaflet library for dynamic map display has significantly improved processing times and removed limitations on zoom levels.

The second part of the article presents the range of earth observation products distributed by HOTVOLC, which has been constantly enriched over the last ten years, particularly in the field of volcanic ash detection and quantification. The service uses several approaches to detect and quantify volcanic ash in clouds. Here we describe in detail the "2-band method", which uses brightness temperature differences to distinguish volcanic ash from other particles, the "3-band method", which is based on the use of Boolean tests on brightness temperature differences of three thermal infrared

channels, the "5-band method", which further refines detection by using additional spectral bands, the "RGB/24-bit" algorithm, which combines three spectral bands into a multispectral RGB image where volcanic ash appears in a specific color, the "ash cloud altitude" product, which provides the altitude at the top of the cloud, the "ash plume mass" product, which represents vertical column densities, and finally the "ash plume contour" product, showing a rough contour line around the cloud.

Finally, we describe the 3 main areas of future development for the HOTVOLC service: [1] improving volcanic ash detection by integrating machine learning techniques. The exploration of supervised and unsupervised learning methods promises significant improvements in decision support for air traffic management, particularly in the area covered by the Toulouse VAAC. [2] The future integration of data from other geostationary satellites, such as GOES-16 and EUMETSAT's Indian Ocean Data Coverage service (IODC), promises to improve product quality for regions with limited spatial resolution. This integration will enable HOTVOLC to significantly improve its capabilities for monitoring active French volcanoes in the Antilles and Reunion Island regions. [3] Finally, the planned transition from METEOSAT second generation to METEOSAT third generation (MTG) should bring significant improvements to the service. Thanks to the advanced capabilities of the Flexible Combined Imager (FCI), including improved acquisition frequency and spatial resolution, HOTVOLC will be better equipped to monitor and study volcanic eruption dynamics in greater detail.

In conclusion, the progress and future prospects of the HOTVOLC service and the recent redesign of its web-GIS interface testify to its commitment to easily provide accurate and timely information for real-time volcanic activity observation and risk management. These advances will undoubtedly enhance the service's capabilities, providing invaluable support to decision-makers, aviation authorities and volcanic risk assessment teams worldwide.

References

Ackermann, S., 1997. Remote sensing aerosols using satellite infrared observations. *Journal of Geophysical Research*, 102(D14), pp.17069-17079. https://doi.org/10.1029/96JD03066

Beckett, F.M., Witham, C.S., Leadbetter, S.J., Crocker, R., Webster, H.N., Hort, M.C., Jones, A.R., Devenish, B.J., Thomson, D.J., 2020. Atmospheric dispersion modelling at the London VAAC: A review of developments since the 2010 Eyjafjallajökull volcano ash cloud. *Atmosphere*, 11(4), p.352. https://doi.org/10.3390/atmos11040352

Casadevall, T.J., 1994a. *Volcanic ash and aviation safety: proceedings of the first international symposium on volcanic ash aviation and safety*. US Government Printing Office

Casadevall, T.J., 1994b. The 1989-1990 eruption of Redoubt Volcano, Alaska: impacts on aircraft operations. *Journal of volcanology and geothermal research*, 62(1-4), pp.301-316. https://doi.org/10.1016/0377-0273(94)90038-8

Casadevall, T.J., Delos Reyes, P.J. & Schneider, D.J., 1996. The 1991 Pinatubo eruptions and their effects on aircraft operations. In *Fire and Mud: eruptions and lahars of Mount Pinatubo, Philippines*. University of Washington Press. pp.625-636

Casadevall, T., Thompson, T. & Fox, T., 1999. *World map of volcanoes and principal aeronautical features*. Map 1-2700. US Geological Survey

Ellrod, G.P. & Connel, B., 1999. Improvements in volcanic ash detection using GOES multi-spectral image data. In *8th Conference on Aviation, Range, and Aerospace Meteorology*. Dallas, TX, 1999. American Meteorological Society

Ellrod, G.P., Connell, B.H. & Hillger, D.W., 2003. Improved detection of airborne volcanic ash using mutlispectral infrared satellite data. *Journal of Geophysical Research: Atmospheres*, 108(D12), https://doi.org/10.1029/2002JD002802

Francis, P.N., Cooke, M.C. & Saunders, R.W., 2012. Retrieval of physical properties of volcanic ash using Meteosat: A case study from the 2010 Eyjafjallajökull eruption. *Journal of Geophysical Research: Atmospheres*, 117(D20), https://doi.org/10.1029/2011JD016788

Furtney, M.A., Pritchard, M.E., Biggs, J., Carn, S.A., Ebmeier, S.K., Jay, J.A., McCormick Kilbride, B.T., Reath, K.A., 2018. Synthesizing multi-sensor, multi-satellite, multi-decadal for global volcano monitoring. *Journal of Volcanology and Geothermal Research*, 365, pp.38-56. https://doi.org/10.1016/j.jvolgeores.2018.10.002

Gong, S. & Newman, T., 2017. Fine feature sensitive marching square. *IET Image Processing*, 11(9), pp.796-802. https://doi.org/10.1049/iet-ipr.2016.1124

Gouhier, M., 2022. Surveillance des volcans par télédétection spatiale. In J.-F. Lénat, ed. *Aléas et surveillance de l'activité volcanique 2 : Sismologie, déformation et télédétection*. ISTE Group. pp.177-226

Gouhier, M., Deslandes, M., Guéhenneux, Y., Hereil, P., Cacault, P., Josse, B., 2020. Operational response to volcanic ash risks using HOTVOLC satellite-based system and MOCAGE-Accident model at the Toulouse VAAC. *Atmosphere*, 11(8), p.864. https://doi.org/10.3390/atmos11080864

Gouhier, M., Guéhenneux, Y., Labazuy, P., Cacault, P., Decriem, J., Rivet, S., 2016. HOTVOLC: a web-based monitoring system for volcanic hot spots. *Geological Society, London, Special Publications*, 426(1), pp.223-241. https://doi.org/10.1144/SP426.31

Gouhier, M., Harris, A., Calvari, S., Labazuy, P., Guéhenneux, Y., Donnadieu, F., Valade, S., 2012. Lava discharge during Etna's January 2011 fire fountain tracked using MSG-SEVIRI. *Bulletin of Volcanology*, 74, pp.787-793. https://doi.org/10.1007/s00445-011-0572-y

Guéhenneux, Y., Gouhier, M. & Labazuy, P., 2015. Improved space borne detection of volcanic ash for real-time monitoring using 3-Band method. *Journal of Volcanology and Geothermal Research*, 283, pp.25-45. https://doi.org/10.1016/j.jvolgeores.2015.01.005

Guffanti, M., Ewert, J.W., Gallina, G.M., Bluth, G.J.S., Swanson, G.L., 2005. Volcanic-ash hazard to aviation during the 2003-2004 eruptive activity of Anatahan volcano, Commonwealth of the Northern Mariana Islands. *Journal of Volcanology and Geothermal Research*, 146(1-3), pp.241-255. https://doi.org/10.1016/j.jvolgeores.2004.12.011

Holmlund, K., Grandel, J., Schmetz, J., Stuhlmann, R., Bojkov, B., Munro, R., Lekouara, M., Coppens, D., Viticchie, B., August, T. et al., 2021. Meteosat Third Generation (MTG): Continuation and Innovation of Observations from Geostationary Orbit. *Bulletion of the American Meteorological Society*, 102(5), pp.E990-E1015. https://doi.org/10.1175/BAMS-D-19-0304.1

ICAO EUR/NAT VACP, 2016. Volcanic ash contingency plan - European and North Atlantic Regions. In *Eur Doc 019-NAT*. Montréal, QC, Canada, 2016. ICAO

International Volcanic Ash Task Force, 2010. Perspective on aircraft airworthiness when operating in airspace containing volcanic ash. In *IVATF First Meeting, 27 to 30 july*. Montréal, QC, Canada, 2010

Labazuy, P., Gouhier, M., Harris, A., Guéhenneux, Y., Hervo, M., Bergès, J.-C., Fréville, P., Cacault, P., Rivet, S., 2012. Near real-time monitoring of the April-May 2010 Eyjafjallajökull ash cloud: an example of a web-based, satellite data-driven, reporting system. *International Journal of Environment and Pollution*, 48(1-4), pp.262-272. https://doi.org/10.1504/IJEP.2012.049673

Lechner, P., Tupper, A., Guffanti, M., Loughlin, S., Casadevall, T., 2018. Volcanic ash and aviation - The challenges of real-time, global communication of a natural hazard. In C.J. Fearnlay et al., eds. *Observing the volcano world. Advances in Volcanology.* Springer, Cham. pp.51-64

Marchese, F., Filizzola, C., Mazzeo, G., Pergola, N., Sannazzaro, F., Tramutoli, V., 2011. Assessment and validation in time domain of a Robust Satellite Technique (RST ash) for ash cloud detection. *Geomatics, Natural Hazards and Risk*, 2(3), pp.247-262. https://doi.org/10.1080/19475705.2011.564211

Miller, T.P. & Casdevall, T.J., 2000. Volcanic ash hazards to aviation. In H. Sigurdsson et al., eds. *Encyclopedia of Volcanoes*. San Diego: Academic Press. pp.915-930

Mosher, F.R., 2000. Four channel volcanic ash detection. In *10th Conference on Satellite Meteorology and Oceanography*. Long Beach, CA, 2000

Pavolonis, M.J., 2010. Advances in extracting cloud composition information from spaceborne infrared radiances - A robust alternative to brightness temperatures. Part I: Theory. *Journal of Applied Meteorology and Climatology*, 49(9), pp.1992-2012. https://doi.org/10.1175/2010JAMC2433.1

Pavolonis, M.J., Feltz, W.F., Heidinger, A.K. & Gallina, G.M., 2006. A daytime complement to the reverse absorption technique for improved automated detection of volcanic ash. *Journal of Atmospheric and Oceanic Technology*, 23(11), pp.1422-1444. https://doi.org/10.1175/JTECH1926.1

Pavolonis, M. & Sieglaff, J., 2012. *GOES-R Advanced Baseline Imager (ABI) algorithm theoretical basis document for volcanic ash (detection and height) - Version 3*. [Online] Available at: https://www.star.nesdis.noaa.gov/goesr/documents/ATBDs/Baseline/ATBD_GOES-R_VolAsh_v3.0_July2012.pdf

Pavolonis, M., Sieglaff, J. & Cintineo, J., 2018. Automated Detection of Explosive Volcanic Eruptions Using Satellite-Derived Cloud Vertical Growth Rates. *Earth And Space Science*, 5, pp.903-928. https://doi.org/10.1029/2018EA000410

Pavolonis, M.J., Sieglaff, J.M. & Cintineo, J.L., 2020. Chapter 10: Remote sensing of volcanic ash with the GOES-R series. In S.J. Goodman, T.J. Schmit, J. Daniels & R.J. Redmon, eds. *The GOES-R Series*. Elsevier. Ch. 10. pp.103-124

Pergola, N., Marchese, F., Tramutoli, V., Filizzola, C., Ciampa, M., 2008. Advanced satellite technique for volcanic activity monitoring and early warning. *Annals of Geophysics*, 1(51), Available at: http://hdl.handle.net/2122/4992

Pergola, N., Pietrapertosa, C., Lacava, T. & Tramutoli, V., 2001. Robust satellite techniques for monitoring volcanic eruptions. *Annals of Geophysics*, 2(44), Available at: http://hdl.handle.net/2122/1205

Pergola, N., Tramutoli, V., Marchese, F., Scaffidi, I., Lacava, T., 2004. Improving volcanic ash cloud detection by a robust satellite technique. *Remote Sensing of Environment*, 90(1), pp.1-22. https://doi.org/10.1016/j.rse.2003.11.014

Platt, C.M. & Prata, A.J., 1993. Nocturnal effects in the retrieval of land surface temperatures from satellite measurements. *Remote Sensing of Envrionment*, 45(2), pp.127-136. https://doi.org/10.1016/0034-4257(93)90037-X

Potts, R.J. & Ebert, E.E., 1996. On the detection of volcanic ash in NOAA AVHRR infrared satellite. In *8th Australian Remote Sensing Conference*. Canberra, 1996

Prata, A.J., 1989a. Observations of volcanic ash clouds in the 10-12 µm window using AVHRR/2 data. *International Journal of Remote Sensing*, 10(4-5), pp.751-761. https://doi.org/10.1080/01431168908903916

Prata, A.J., 1989b. Infrared radiative transfer calculations for volcanic ash clouds. *Geophysical Research Letters*, 16(11), pp.1293-1296. https://doi.org/10.1029/GL016i011p01293

Prata, A.J., 2009. Satellite detection of hazardous volcanic clouds and the risk to global air traffic. *Natural hazards*, 51, pp.303-324. https://doi.org/10.1007/s11069-008-9273-z

Prata, F., Bluth, G., Rose, B., Schneider, D., Tupper, A., 2001. Comments on "Failures in detecting volcanic ash from a satellite-based technique". *Remote Sensing of Environment*, 78(3), pp.341-346. https://doi.org/10.1016/S0034-4257(01)00231-0

Prata, A.J. & Grant, I.F., 2001. Retrieval of microphysical and morphological properties of volcanic ash plumes from satellite data: Application to Mt Ruapehu, New Zealand. *Quarterly Journal of the Royal Meteorological Society*, 127(576), pp.2153-2179. https://doi.org/10.1002/qj.49712757615

Prata, A.J. & Kerkmann, J., 2007. Simultaneous retrieval of volcanic ash and SO2 using MSG-SEVIRI measurements. *Geophysical Research Letters*, 34(5), https://doi.org/10.1029/2006GL028691

Prata, A.J. & Tupper, A., 2009. Aviation hazards from volcanoes: the state of science. *Natural hazards*, 51(2), pp.239-244. https://doi.org/10.1007/s11069-009-9415-y

Rix, M., Valks, P., Hao, N., Van Geffen, J., Clerbaux, C., Clarisse, L., Coheur, P.-F., Loyola R., D.G., Erbertseder, T., Zimmer, W. et al., 2009. Satellite monitoring of volcanic sulfur dioxide emissions for early warning of volcanic hazards. *IEEE Journal of Selected Topics in Applied Earth Observations and Remote Sensing*, 2(3), pp.196-206. https://doi.org/10.1109/JSTARS.2009.2031120

Rose, W., Bluth, G., Schneider, D., Ernst, G., Riley, C., Henderson, L., McGimsey, R., 2001. Observations of Volcanic Clouds in Their First Few Days of Atmospheric Residence: The 1992 Eruptions of Crater Peak, Mount Spurr Volcano, Alaska. *The Journal of Geology*, 109(6), pp.677-694. https://doi.org/10.1086/323189

Schmetz, J., Pili, P., Tjemkes, S., Just, D., Kerkmann, J., Rota, S., Ratier, A., 2002. SEVIRI Calibration. *Bulletin of the American Meteorological Society*, 83(7), pp.ES52-ES53

Schultz, C., 2012. Fine aspherical ash source of Eyjafjallajökull's influence. *Eos, Transactions American Geophysical Union*, 93(10), pp.116-116. https://doi.org/10.1029/2012EO100016

Scollo, S., Prestifilippo, M., Spata, G., D'Agostino, M., Coltelli, M., 2009. Monitoring and forecasting Etna volcanic plume. *Natural Hazards and Earth System Sciences*, 9(5), pp.1573-1585. https://doi.org/10.5194/nhess-9-1573-2009

Simpson, J.J., Hufford, G., Pieri, D. & Berg, J., 2000. Failures in detecting volcanic ash from a satellite-based technique. *Remote Sensing of Environment*, 72(2), pp.191-217. https://doi.org/10.1016/S0034-4257(99)00103-0

Tramutoli, V., 1998. Robust AVHRR techniques (RAT) for environmental moniotring: theory and applications. In *Earth surface remote sensing II*. Barcelona, Spain, 1998. SPIE

Watkin, S., 2003. The application of AVHRR data for the detection of volcanic ash in a Volcanic Ash Advisory Centre. *Meteorological Applications*, 10(4), pp.301-311. https://doi.org/10.1017/S1350482703001063

Wen, S. & Rose, W., 1994. Retrieval of sizes and total masses of particles in volcanic clouds using AVHRR bands 4 and 5. *Journal of Geophysical Research*, 99(D3), pp.5421-5431. https://doi.org/10.1029/93JD03340

Wright, R. & Flynn, L.P., 2003. On the retrieval of lava-flow surface temperatures from infrared satellite data. *Geology*, 31(10), pp.893-896. https://doi.org/10.1130/G19645.1

Yu, T., Rose, W.I. & Prata, A.J., 2002. Atmospheric correction for satellite-based volcanic ash mapping and retrievals using "split window" IR data from GOES and AVHRR. *Journal of Geophysical Research: Atmopsheres*, 107(D16), pp.AAC 10-1-AAC 10-19. https://doi.org/10.1029/2001JD000706

Figures captions

Fig. 1 Spatial extents of volcanic zones monitored by the HOTVOLC system. The dashed line represents the MSG-SEVIRI spatial coverage. [1] Iceland, [2] France, [3] Italy-Greece, [4] African Rift, [5] East Africa, [6] Comoros, [7] Reunion Island, [8] Cameroon, [9] Cape Verde, [10] Canary Islands, [11] Azores, [12] West Indies

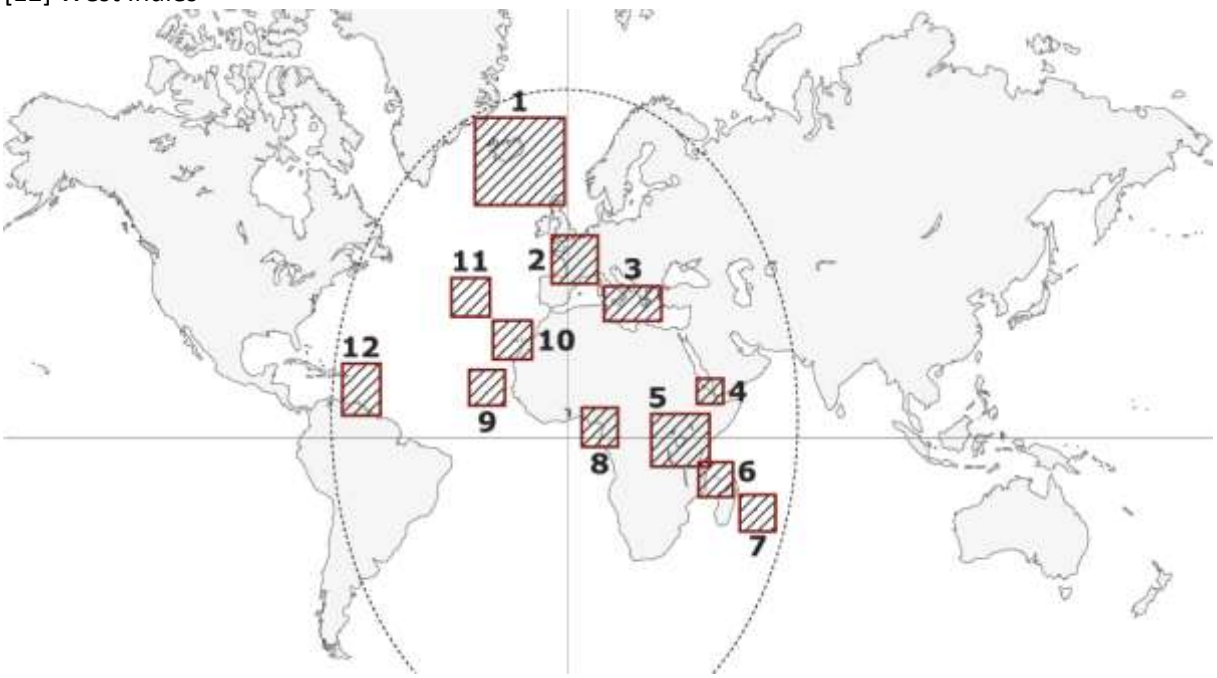

Fig. 2 Screenshot of the old V2 web-GIS interface of the HOTVOLC service used for the last 10 years (a) selection of products (b) navigation in time using the calendar (c) Fagradalsfjall volcano marker in yellow indicating moderate volcanic activity on 11 July 2023 at 12:00 (d) access to time series

Fig. 3 Screenshot of the new HOTVOLC web-GIS interface V3.0 in the operational, or real-time, mode

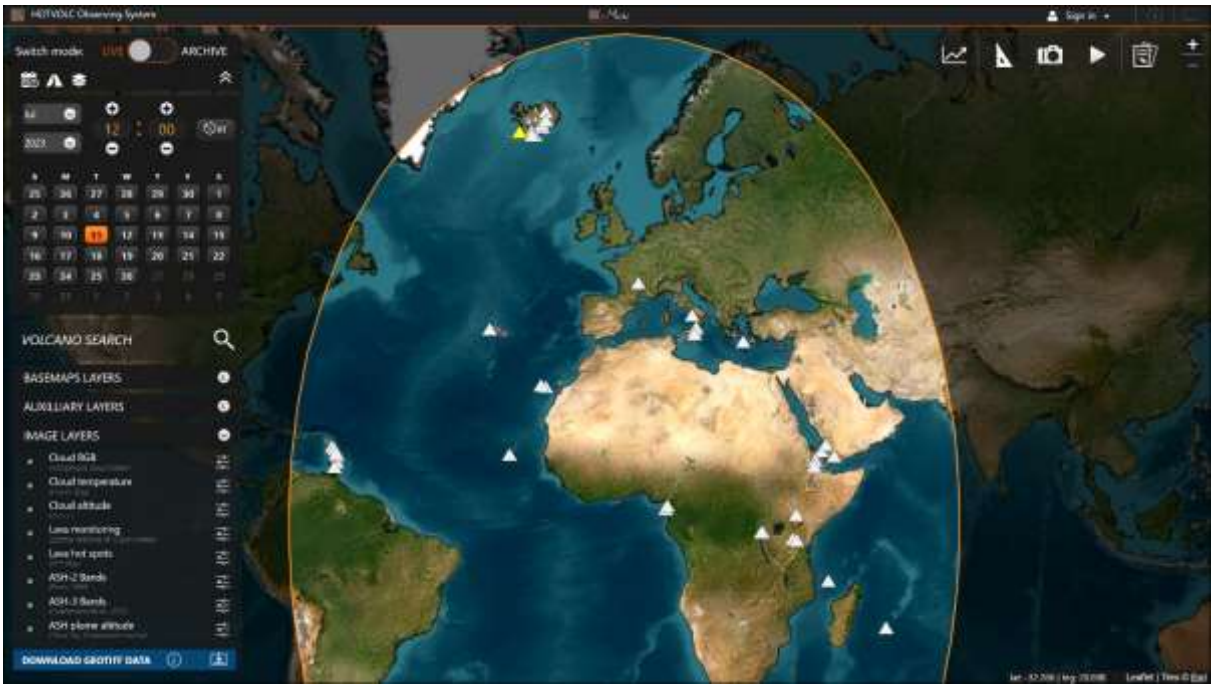

Fig. 4 Screenshot of the new HOTVOLC web-GIS v3.0 interface in archive mode (a) the advanced search form to explore eruption database (b) the results table showing all eruptions matching the search parameters

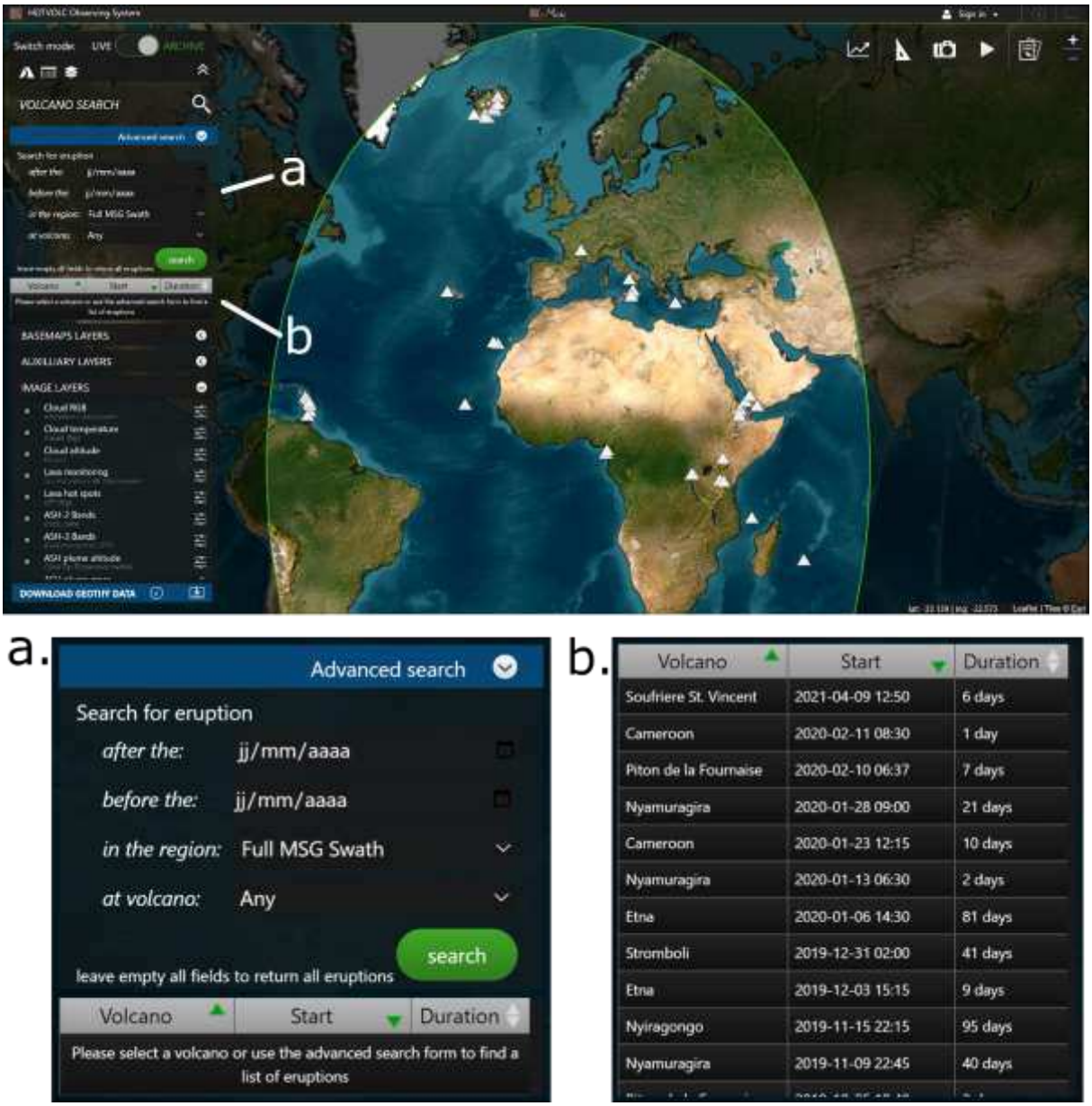

Fig. 5 Screenshot of the new HOTVOLC web-GIS v3.0 interface in archive mode during the exploration of the Fogo eruption of 23 November 23 2014. At the bottom of the figure a zoom on the time navigation system (a) the date and time form field (b) buttons to increment or decrement the time (c) the timeline where the green horizontal bar represents the temporal extent of the eruption and the red vertical bar the currently displayed date

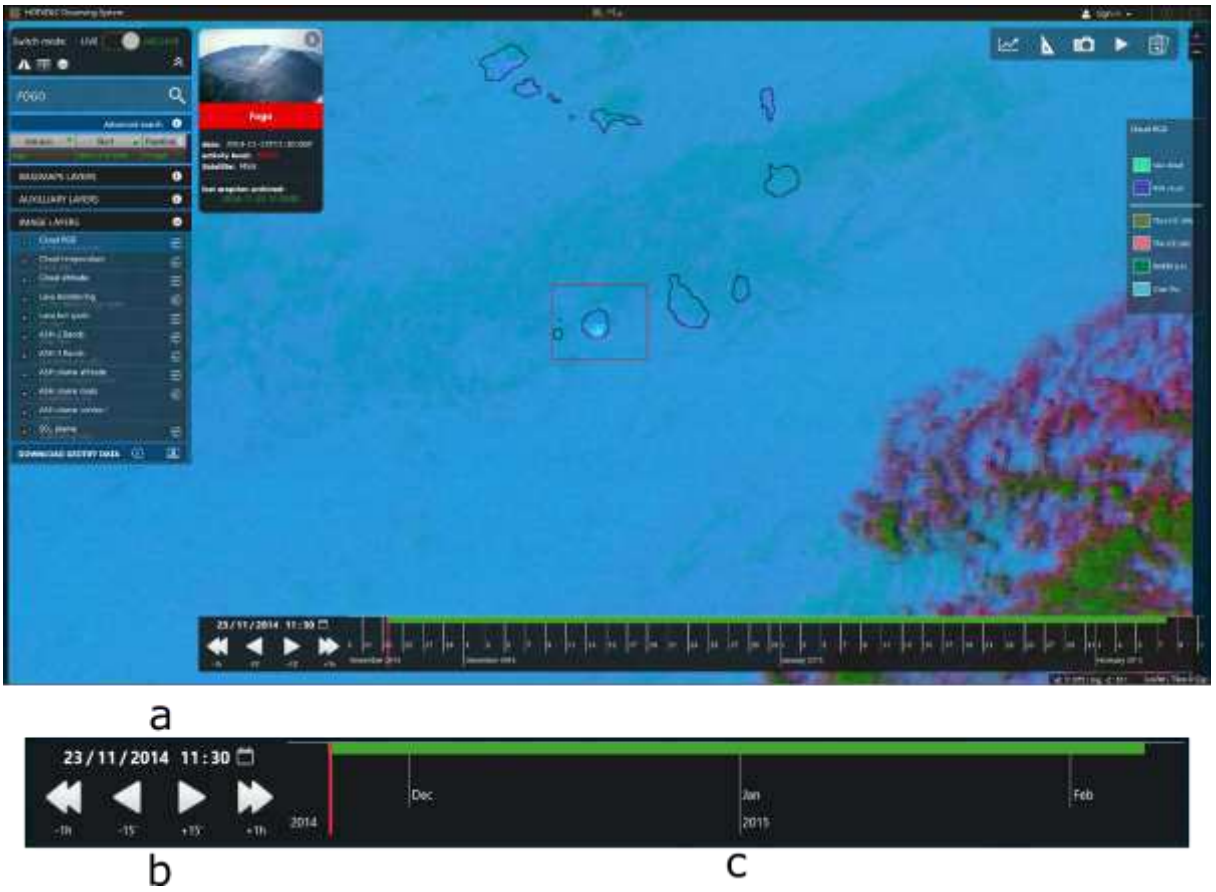

Fig. 6 Example of using the new GIS features to measure the area of the SO2 plume during the eruption of the Fogo volcano on 24 November 2014 at 10:15. On the left part of the figure is the menu of GIS functionalities with from top to bottom: (a) toggle display of distance and area measures, (b) editing style of drawing, (c) add a marker, (d) draw a polyline, (e) draw a rectangle, (f) draw a polygon, (g) draw a circle, (h) add a circle marker, (i) add text area, (j) edit drawing nodes, (k) move layers, (l) cut layers, (m) delete layers, (n) rotate layers

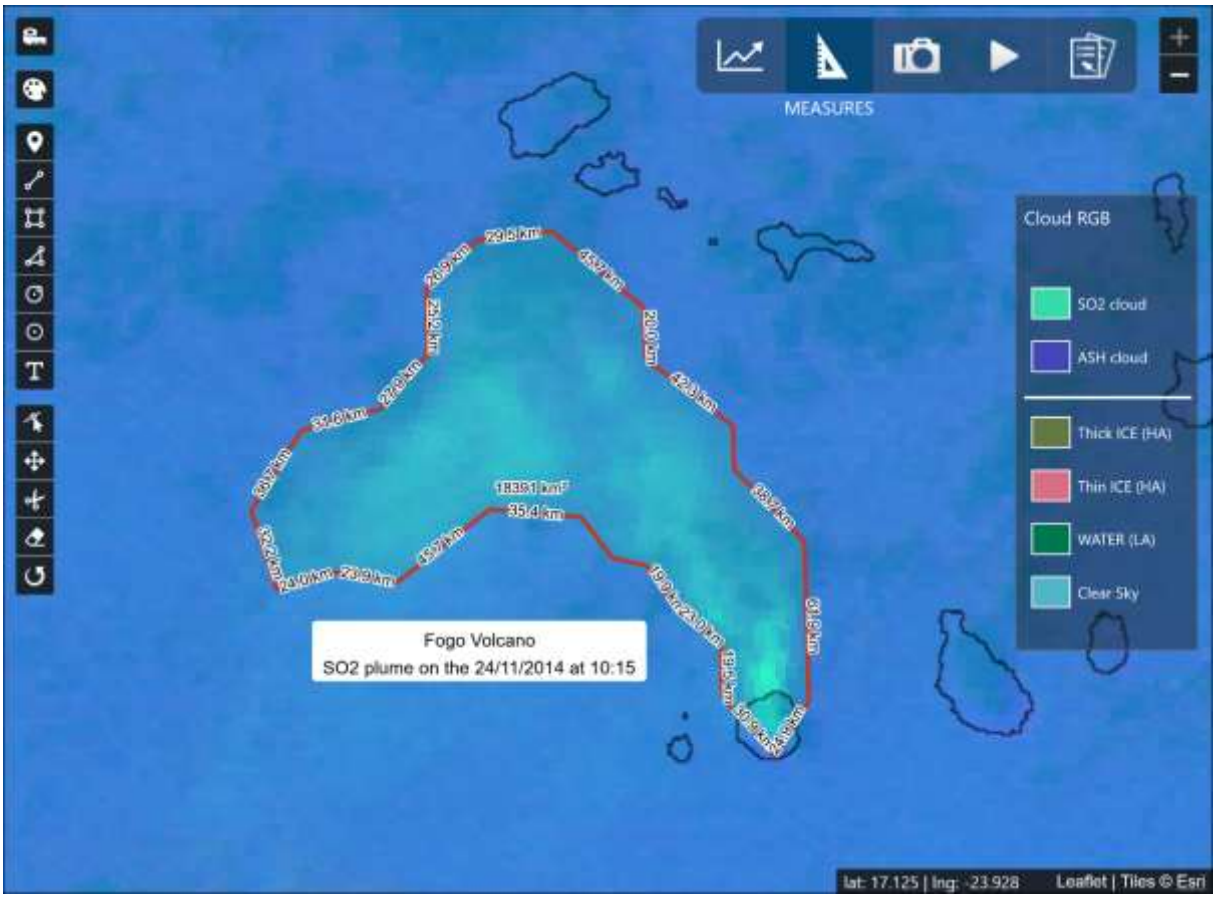

Fig. 7 Maps of ash cloud detected during the 17 April 2010 Eyjafjallajökull eruption at 16:00 UTC with the (a) RGB product (ash cloud appears in dark blue), and the brightness temperature difference (in K) using (b) 2-band, (c) 3-band, (d) 5-band methods, respectively

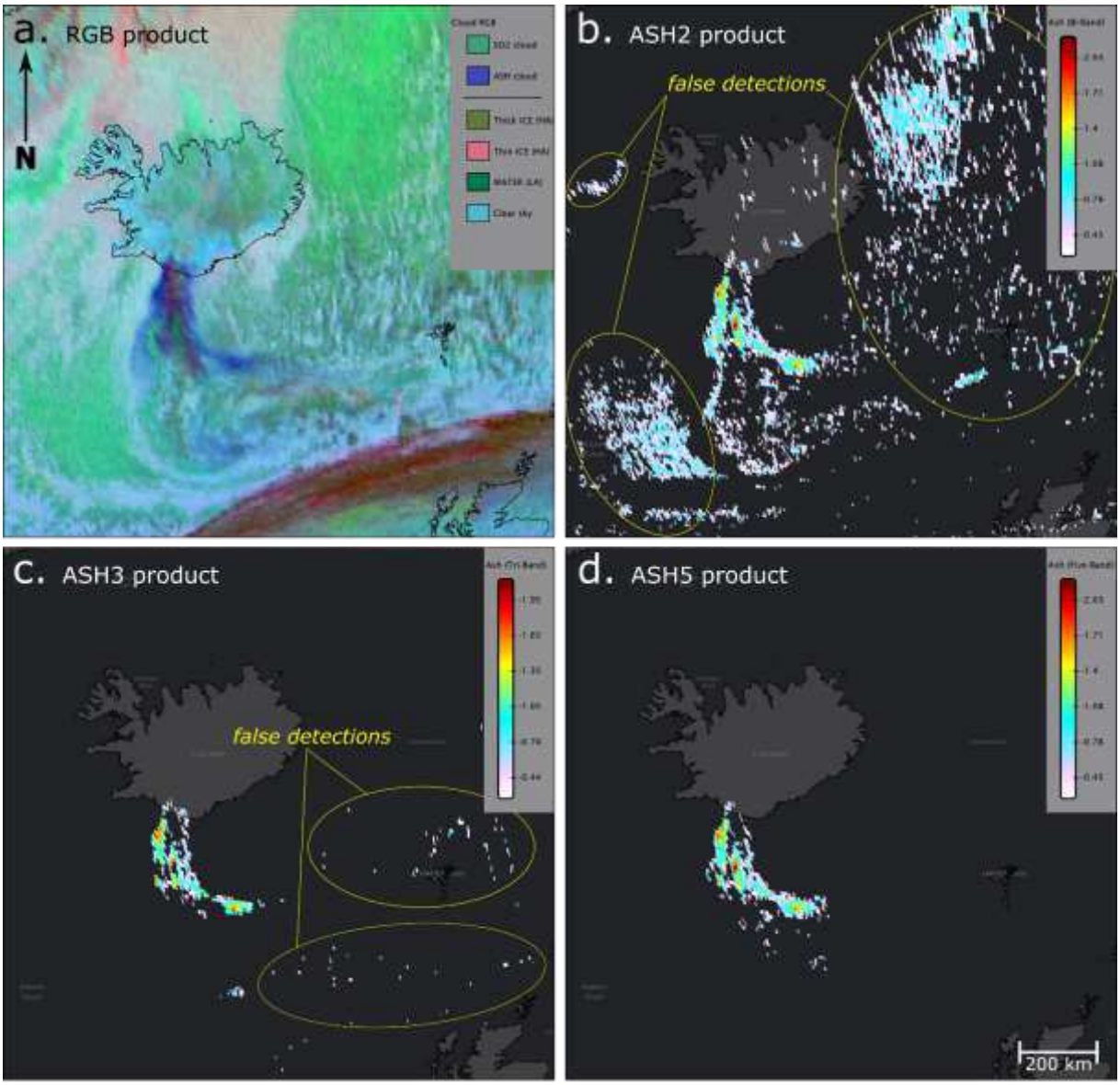

Fig. 8 *(a)* RGB composite image using 3 spectral band (8.7, 10.8 and 12 µm) revealing dark blue pixels highlighting the presence of volcanic ash during the 23 May 2021 Nyiragongo eruption at 08:30 UTC. (b) Pixels containing ash, i.e., those that pass all the tests (B/G>2, R<100 and G<100), are identified by the color yellow.

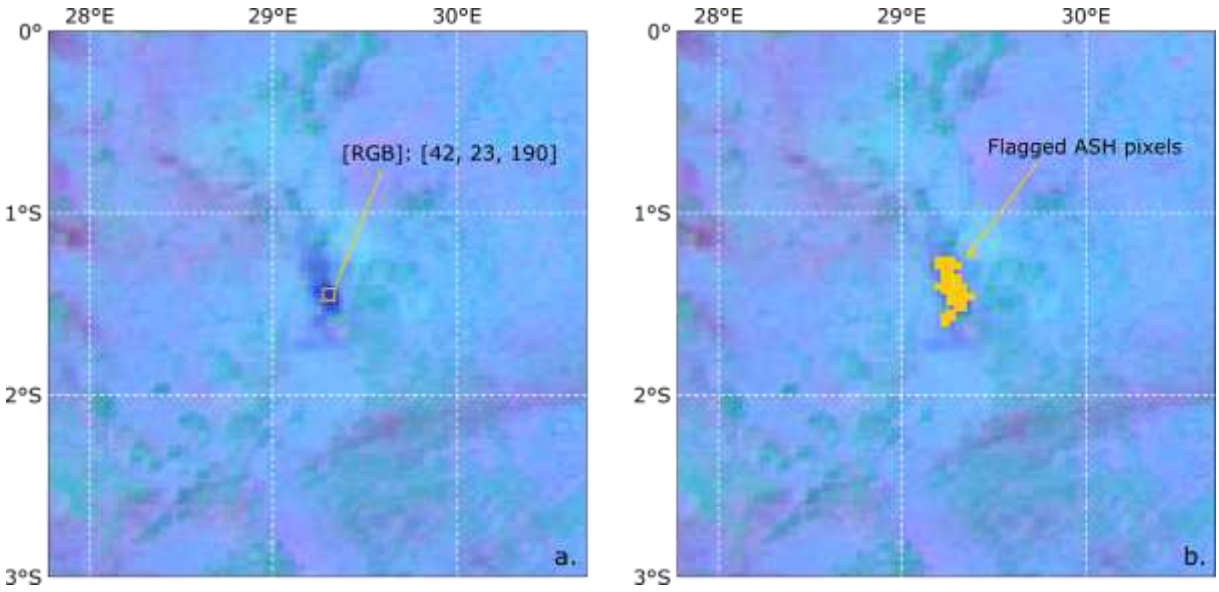

Fig. 9 Time series of ash mass loading (grey line) in the volcanic plume during the May-July 2021 eruption of Nyiragongo, with a 1-hour moving average (red line).

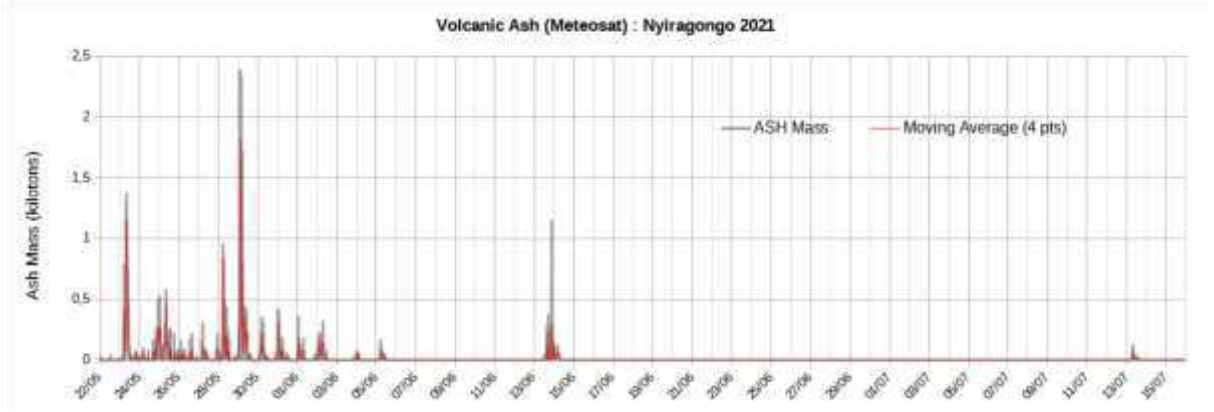

Fig. 10 Ash cloud satellites products provided by HOTVOLC system during the 17 April 2010 eruption of Eyjafjallajökull at 16:00 UTC showing (a) the cloud contour, (b) the top ash cloud altitude (in km), (c) the vertical column density a measure of the ash loading in the cloud (in g/m^2)

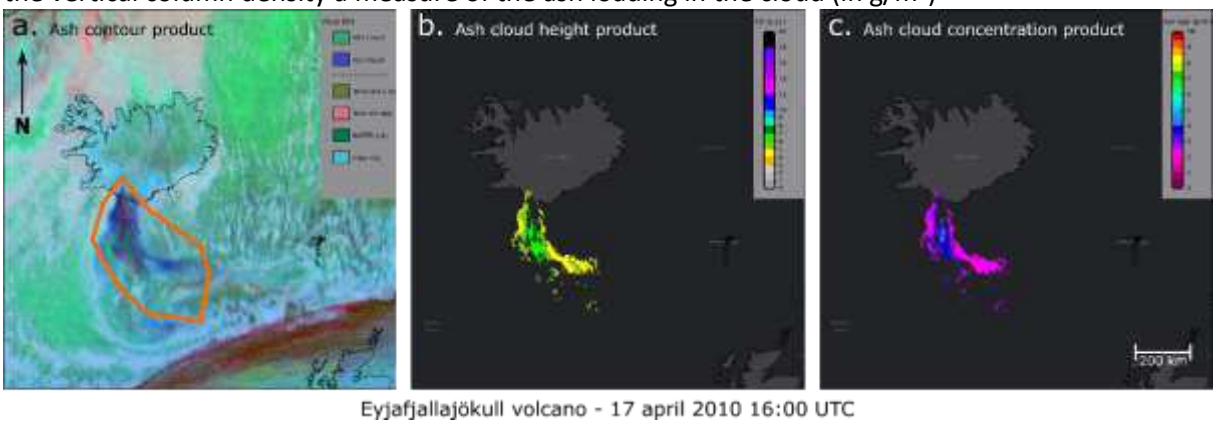

Fig. 11 (a) Boolean 2D array from ash detection via the 2-band algorithm, (b) Isoline calculated from the marching square method separating ash-free areas from contaminated ones, (c) Convex hull calculated around isolines with a 3 pixel buffer

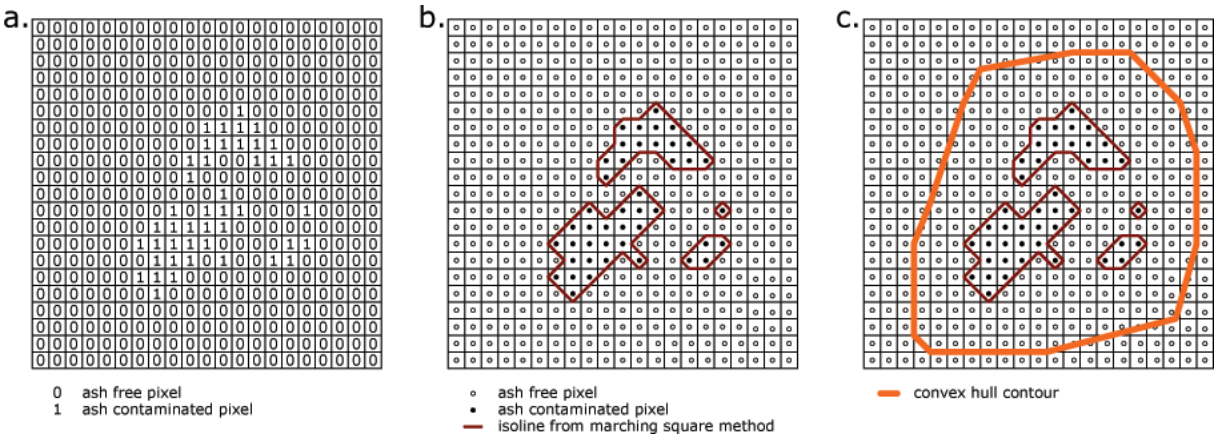

Fig. 12 Volcanic ash clouds during the eruption of Soufrière St Vincent on 10 April 2021 at 13:00 UTC. (upper part of the figure) Imaged by MSG and visible in the V2 interface, the ash appears in dark blue, (lower part of the figure) Imaged by GOES and visible in the archive mode of the V3 interface, here because differences in spectral bands available between GOES and MSG the colored composition is not identical and the ash appears in red

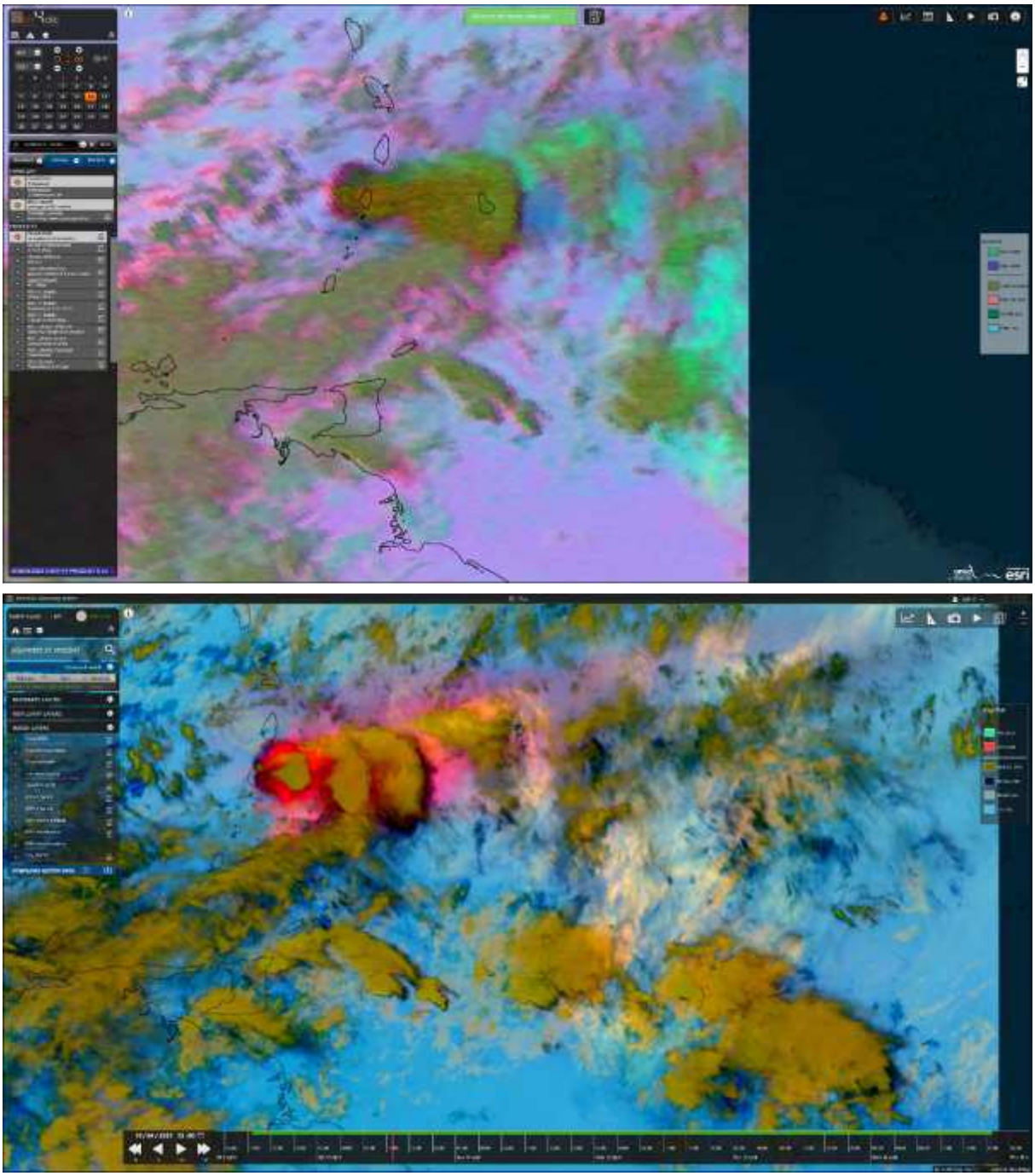

Tables captions

Table 1 CCT technique look-up table cloud altitude versus cloud temperature function of the latitude region and the season

Altitude	Mid-latitude region			Tropical region
	Winter	Mid-Season	Summer	
Km	*K*	*K*	*K*	*K*
0	272.20	283.20	294.20	299.70
1	268.70	279.20	289.70	293.70
2	265.20	275.20	285.20	287.70
3	261.70	270.45	279.20	283.70
4	255.70	264.45	273.20	277.00

5	249.70	258.45	267.20	270.30
6	243.70	252.45	261.20	263.60
7	237.70	246.20	254.70	257.00
8	231.70	239.95	248.20	250.30
9	225.70	233.70	241.70	243.60
10	219.70	227.50	235.30	237.00
11	219.20	224.00	228.80	230.10
12	218.70	220.50	222.30	223.60
13	218.20	217.00	215.80	217.00
14	217.70	216.72	215.75	210.30
15	217.20	216.45	215.70	203.70
16				197.00
17				194.80